(This is a sample cover image for this issue. The actual cover is not yet available at this time.)

Earth and Planetary Science Letters 319-320 (2012) 75–82

Contents lists available at SciVerse ScienceDirect

Earth and Planetary Science Letters

journal homepage: www.elsevier.com/locate/epsl

From superchrons to secular variation: A broadband dynamo frequency spectrum for the geomagnetic dipole

Peter L. Olson [a,*], Ulrich R. Christensen [b], Peter E. Driscoll [c]

[a] Department of Earth and Planetary Sciences, Johns Hopkins University, Baltimore, MD 21218, USA
[b] Max Planck Institute for Solar System Research, Katlenburg-Lindau, Germany
[c] Department of Geology and Geophysics, Yale University, New Haven CT, USA

ARTICLE INFO

Article history:
Received 6 September 2011
Received in revised form 21 November 2011
Accepted 3 December 2011
Available online xxxx

Editor: Y. Ricard

Keywords:
geodynamo
geomagnetic spectrum
dipole variations
Earth's core

ABSTRACT

We build a broadband frequency spectrum for geomagnetic dipole intensity variations originating in the core using results from numerical dynamos. Scaling dipole intensity spectra from numerical dynamos with diverse input parameters (Ekman, Rayleigh, and magnetic Prandtl numbers) and magnetic Reynolds numbers from 170 to 1985 yields a composite spectrum ranging from ultra-low frequencies (~100 Myr period) to very high frequencies (~1 yr period). The amplitude and shape of our composite spectrum compare favorably with estimates of the geomagnetic and paleomagnetic dipole moment spectra. Significant power is found in an ultra-low frequency band $f<0.1$ Myr^{-1} that corresponds to geomagnetic superchrons and also in a low frequency band $f=0.1-5$ Myr^{-1} that corresponds to the time scales of geomagnetic polarity chrons. In higher frequency bands our composite spectrum varies with frequency approximately like f^{-n}. In a transitional frequency band from $f=5$ Myr^{-1} to $f=2$ kyr^{-1}, characteristic of relative paleointensity variations in sediments, we find $n\simeq 1.8$. In a high frequency band with $f>2$ kyr^{-1}, representing archaeomagnetic and historical geomagnetic secular variation, we find $n\simeq 4$ on average, with spectral slope increasing at very high frequencies to near $n\simeq 6$ at $f=1$ yr^{-1}. The secular variation and the secular acceleration spectra for the dipole field reach their peak values in the high frequency band, close to frequencies where spectra for the dynamo fluid velocity decrease sharply.

1. Introduction

Dynamo processes within the Earth's core induce time variations of the geomagnetic dipole moment that range over ten orders of magnitude in frequency. The lowest frequency band involves variability with periodicities longer than 100 Myr, evident in the time interval between geomagnetic superchrons, for example. Such ultra-low frequency variability might be due to the thermal evolution of the core-mantle system (Aubert et al., 2009; Driscoll and Olson, 2011; Glatzmaier et al., 1999), whereas higher frequency fluctuations of the geomagnetic dipole are usually assumed to reflect intrinsic dynamo processes. The highest frequency dipole moment fluctuations with a geodynamo origin may correspond to the inertial wave frequency in the outer core, although such short-term variations are expected to be strongly filtered by the electrical conductivity of the mantle and have not yet been observed. However, sub-annual variations of the dipole intensity relative to its historical downward trend have been observed in the secular variation of the core field (Jackson et al., 2000; Olsen et al., 2005).

Measurements of the relative geomagnetic field intensity derived from sediment cores and other paleomagnetic methods commonly show large amplitude variations, even in global stacks (Guyodo and Valet, 1999; Valet et al., 2005). Frequency spectra calculated by converting these intensity variations to dipole moment variations (Constable and Johnson, 2005; Courtillot and Le Mouel, 1988; Ziegler et al., 2011) reveal that much of the power (variance) in geomagnetic dipole intensity fluctuations is distributed over broad frequency bands that correspond to time scales that are far longer than those usually associated with dynamical processes in the outer core, such as the convective turnover time, which is of the order of a few centuries, or the dipole free decay time, which is of the order of a few hundred centuries. In addition, the geomagnetic spectrum does not follow a power-law with a constant exponent n over its entire frequency range. For example, the geomagnetic dipole moment spectrum developed by Constable and Johnson (2005) shows discrete bands at ultra-low and low frequencies with very small n-values that correspond to polarity superchron and polarity chron time scales, respectively, an intermediate or transitional band with an increasingly negative slope that corresponds to the time scales of paleomagnetic secular variation, and a high frequency band with a very large negative slope corresponding to the time scales of the archaeomagnetic and historical geomagnetic records. Fits to the geomagnetic spectrum

* Corresponding author.
E-mail address: olson@jhu.edu (P.L. Olson).

0012-821X/$ – see front matter © 2011 Elsevier B.V. All rights reserved.
doi:10.1016/j.epsl.2011.12.008

with the form $\mathcal{S} \propto f^{-n}$, where $\mathcal{S}$ is the spectral variance and f is frequency in cycles per unit time, typically yield $n \simeq 2$ in the intermediate or transitional band (Barton, 1982; Courtillot and Le Mouel, 1988) and $n \geq 11/3$ in the high frequency band (Consolini et al., 2002; Curie, 1968).

Numerical dynamos that are run long enough to produce their full range of variability, including reversals and excursions, show broadband frequency spectra for magnetic field intensity and also for fluid velocity (Driscoll and Olson, 2009; Sakuraba and Hamano, 2007; Tanriverdy and Tilgner, 2011). The structure of the dipole intensity frequency spectrum can provide information on dynamo processes such as convective turnover time, core-mantle interactions, and oscillations in the core. For example, Sakuraba and Hamano (2007) fit dipole moment spectra from numerical dynamos with Ekman number $E = 1 \times 10^{-5}$ and (thermal) Rayleigh number $Ra = 4 \times 10^{7}$ to power-laws with exponents $n \simeq 5/3$ and $n \simeq 11/3$ over frequencies ranging from $f = 0.05$ kyr^{-1} to $f = 5$ kyr^{-1}, the frequency in their study being defined in terms of the magnetic diffusion time scale. Sakuraba and Hamano (2007) determine that the slope break between these two segments of the dipole spectrum occurs at a frequency near $f = 0.5$ kyr^{-1} in their dynamos, and corresponds to a peak in the spectrum of the azimuthal component of the electric current density below the core-mantle boundary, which they use to define an overturn time scale of about 2 kyr for convection in the core.

These points of similarity between measured geomagnetic dipole frequency spectra and the dipole spectrum from individual numerical dynamos suggest it is feasible to build a more general model for the geomagnetic field spectrum by combining dynamo model results over a wider frequency range. There are practical problems in doing this, however. First, all numerical dynamos lie very far from the Earth in terms of their input parameter values (Christensen and Aubert, 2006; Olson and Christensen, 2006) so there is ambiguity in how to properly scale time and frequency when applying numerical dynamos to the Earth. In addition, the closer a numerical dynamo is to Earth parameters, the shorter its simulation time (Kageyama et al., 2008; Sakuraba and Roberts, 2009) and the narrower its frequency band.

In this paper we propose a method for stacking and scaling frequency spectra from numerical dynamos with diverse input parameters. Applying this method to a suite of numerical dynamos that span the plausible range of magnetic Reynolds numbers for the core, we show that frequency defined using the advection time is the better scale for numerical dynamo spectra, particularly at high frequency. We then use the dynamo results to derive a composite power-law model for the dipole spectrum of the core field over eight orders of magnitude in frequency.

2. Numerical dynamo parameters

We consider numerical dynamos in rotating spherical fluid shells with the geometry of Earth's outer core, driven primarily by compositional convection originating at the inner boundary. Table 1 summarizes the dynamo cases used in this study in terms of their Ekman number E, Rayleigh number Ra, magnetic Prandtl number Pm, run duration based on the number of free decay times for the dipole field, the resulting rms dipole field intensity, and magnetic Reynolds number Rm based on the rms fluid velocity. The Ekman number is defined here as

$$E = \frac{\nu}{d^2 \Omega} \tag{1}$$

where ν and Ω are the kinematic viscosity of the fluid and angular velocity of rotation, respectively, and $d = r_o - r_i$ is the fluid thickness in terms of r_o and r_i, the outer and inner radii, respectively. Our model Rayleigh number is defined as

$$Ra = \frac{g_o F_i d^2}{\kappa^2 \rho \nu} \tag{2}$$

where g_o, F_i, ρ and κ are outer boundary gravitational acceleration, anomalous mass flux due to release of light elements and heat at the inner boundary, fluid density, and thermal diffusivity, respectively. Other control parameters include the Prandtl number and the magnetic Prandtl number, which are

$$Pr = \frac{\nu}{\kappa}, \tag{3}$$

and

$$Pm = \frac{\nu}{\eta}, \tag{4}$$

respectively, where $\eta = 1/\mu_0 \sigma$ is the magnetic diffusivity written in terms of the permeability μ_0 and the electrical conductivity σ. All of the dynamos in Table 1 use $Pr = 1$ and no-slip velocity boundary conditions at both boundaries. Dynamo case *a* assumes the electrical conductivity of the solid inner core is constant and equal to that in fluid. Cases *b*–*g* assume an electrically insulating inner core, set the buoyancy flux at the outer boundary to zero, and fix the local buoyancy flux at the inner boundary at $F_i/4\pi r_i^2$, which corresponds to pure compositional convection with a uniform compositional flux on the inner boundary. Case *a* assumes a uniform light element concentration boundary condition at the inner boundary, with spatially uniform but time variable buoyancy flux at the outer boundary, representing time variations in heat flow out of the core (Driscoll and Olson, 2011). For this case the initial superchron (non-reversing) dynamo stage corresponds to purely compositional convection with zero buoyancy flux at the outer and an initial buoyancy flux of F_i at the inner boundaries, respectively. The buoyancy flux at the outer boundary is then increased to a maximum of about 25% of F_i at the midpoint of the simulation, producing a frequently reversing dynamo state, and then decreased back to zero at the same rate, returning the dynamo to superchron conditions. The Rayleigh number for case a in Table 1 corresponds to a time average of this parameter over one such superchron cycle.

Two important dimensionless output parameters are the magnetic Reynolds number Rm for the rms fluid velocity, and B_{dip}, the rms dipole magnetic field strength on the outer boundary. In terms of dimensional quantities, these are given by

$$Rm = \frac{Ud}{\eta}, \tag{5}$$

Table 1
Dynamo cases summary. E = Ekman number; Ra = Rayleigh number; Pm = magnetic Prandtl number; Rm = magnetic Reynolds number; Trunc. = spherical harmonic truncation; Time = simulation time in dipole decay times; Revs. = polarity reversal count; B_{dip} = dimensionless rms dipole intensity on the outer dynamo boundary (mean, standard deviation).

Case	E	Ra	Pm	Rm	Trunc.	Time	Revs.	B_{dip}
a	5.5×10^{-3}	$2\times10^{+6}$	20	170	42	10000	400	0.59 ± 0.24
b	3×10^{-4}	$3\times10^{+7}$	3	184	64	400	0	0.357 ± 0.08
c	3×10^{-4}	$7\times10^{+7}$	3	375	85	278	5	0.193 ± 0.087
d	1×10^{-4}	$5\times10^{+8}$	2	440	106	5.85	0	0.322 ± 0.045
e	1×10^{-5}	$1\times10^{+11}$	0.8	914	168	0.145	0	0.321 ± 0.027
f	3×10^{-5}	$5\times10^{+9}$	2.5	1030	168	0.4	0	0.222 ± 0.046
g	3×10^{-5}	$5\times10^{+9}$	5	1985	168	0.13	0	0.243 ± 0.056

and

$$B_{dip} = \left(\frac{2\sigma}{\rho\Omega}\right)^{1/2}\left(\frac{\mu_0 m}{4\pi r_o^2}\right) \quad (6)$$

where U is the rms fluid velocity and m is the dipole moment.

The dynamo cases in Table 1 were chosen on the basis of satisfying the "Earth-like" criteria proposed by Christensen et al. (2010) in terms of their magnetic field structure, while at the same time representing a wide range of dynamical conditions. No a-priori consideration was given as to whether or not their frequency spectrum was like the geomagnetic frequency spectrum, and indeed, some of the models we chose show very different time histories. For example, case *c* shown in Fig. 1 has been run for 278 dipole free decay times and reversed its polarity five times, whereas, case *b* with a lower Rayleigh number but otherwise identical parameters did not reverse during 400 dipole free decay times. Simulation time varies inversely with model size, so that in general the low resolution models (corresponding to lower *Rm*-values and large *E*-values) were run for considerably longer simulation times than high resolution models, which have larger *Rm*-values and smaller *E*-values. The longest simulation is case *a*, run for 10,000 decay times with about 400 reversals and two portions of constant polarity superchrons. These long simulations show the irregular, large amplitude variations in total field intensity and dipole field intensity seen in Fig. 1 with polarity reversals and excursions taking place at times of dipole minima. The shorter simulation cases include just a few cycles of the fluctuations seen in Fig. 1 and were too short to find reversals, but because they have larger *Rm*-values their dipole intensity shows more high frequency variability than the lower *Rm* cases.

3. Time and frequency scaling

A major challenge is to compare the spectra of dynamos with short simulation times and large *Rm* with spectra from dynamos with long simulation times and lower *Rm*. In general it is necessary to properly scale both the amplitude and the frequency of each spectrum before comparing one dynamo to another or to the geomagnetic spectrum. Referring to the dynamos in Table 1, we note that among the dynamos run for comparable times, the variances of the dipole intensity are roughly comparable and so are the mean (time average) dipole intensities. Restricting attention to dynamos with the comparable means and variances simplifies the inter-comparison by eliminating the need to re-scale their individual spectral amplitudes, and it also simplifies the comparison of model spectra with the geomagnetic spectrum, since the scale factors for this comparison involve just the means and the standard deviations of their respective dipole moments. Although the means and standard deviations of the dipole intensities B_{dip} in Table 1 are not identical, they are similar enough to justify omitting a separate re-scaling of the amplitude for each dynamo case.

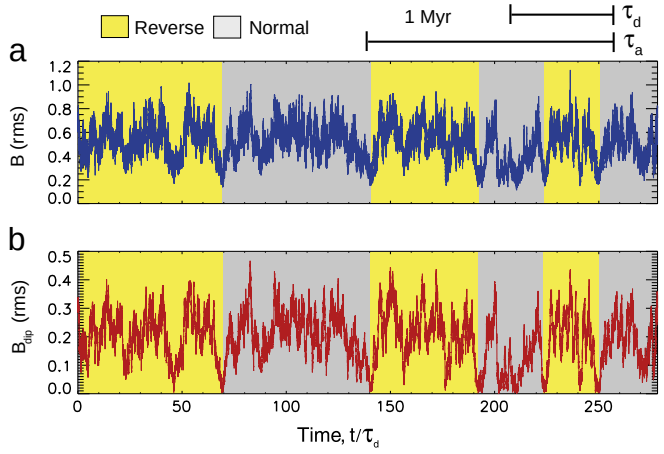

Fig. 1. Time series of (a) rms total field intensity and (b) rms dipole field intensity, both on the outer boundary, for dynamo case *c* with $Rm = 375$ in dipole decay time units (diffusive time scaling). Scale bars denote 1 Myr in the core assuming $\tau_d = 20$ kyr for the dipole decay time and $\tau_a = 90$ yr for the advective time, respectively. Background shading indicates the dipole polarity.

The situation is different for the frequencies, however, because the time scales of the dynamos in Table 1 are vastly different. Our dynamos include several fundamental time scales, including the rotation period, the free decay time of the magnetic field governed by the magnetic diffusivity and represented by the dipole free decay time, the viscous and chemical diffusion times (equal in these dynamos), and an advective time scale related to the convective overturn time. The rotation period of the dynamos in Table 1 is unrealistically long, but this time scale has only an indirect influence on the dipole variations we are considering here, while the chemical and viscous diffusion times are interrelated, each being proportional to the dipole decay time through the magnetic Prandtl number *Pm*. Accordingly, one plausible choice for the time scaling related to frequency is based on the dipole free decay time

$$\tau_d = \frac{r_o^2}{\pi^2\eta}, \quad (7)$$

which we term diffusive time scaling, and a second choice is based on the advection time of the fluid motion, defined by

$$\tau_a = \frac{d}{U}, \quad (8)$$

which we term advective time scaling. These two are related by

$$\tau_d = Rm\left(\frac{r_o}{\pi d}\right)^2 \tau_a. \quad (9)$$

Denoting the dimensional frequency in units of cycles/time by f, the corresponding dimensionless frequencies are $f_a = \tau_a f$ and $f_d = \tau_d f$, respectively. The very large differences implied by these alternatives are evident in Fig.1, which shows scale bars corresponding to 1 Myr of time as defined by (7) and (8) for typical outer core parameter values. In the following section, we determine which of these dimensionless frequencies does a better job of scaling the dynamo spectra.

4. Dynamo frequency spectra for the dipole field

We calculate power spectra from the time series of B_{dip}, the rms dipole intensity on the outer boundary for each dynamo model in Table 1 using the Welch (1967) method with six overlapping Hanning windows equal to one-half of the record length. We then apply smoothing filters to the resulting spectra that consist of running averages of length 3, 7, 11, and 15 points to successive quarter-length segments of each spectrum. For each spectrum, the dimensionless frequencies are assigned according to (7) and (8), and the amplitude of the re-scaled spectra are then adjusted so that the total variance of the original time series is preserved.

Fig. 2 shows the dipole spectra of all the dynamos in Table 1 with the diffusive time scaling applied to the frequencies, and Fig. 3 shows the dipole spectra with the advective time scaling applied to the frequencies, each case labeled by its magnetic Reynolds number *Rm*. It is clear from the comparison of the two figures that the advective time scaling does a better job of stacking the spectra, especially in the higher frequency bands. Fig. 2 shows that the diffusive time scaling disperses the high frequency portions of the spectra in echelon order of their *Rm*-values. In contrast, the high frequency portions of

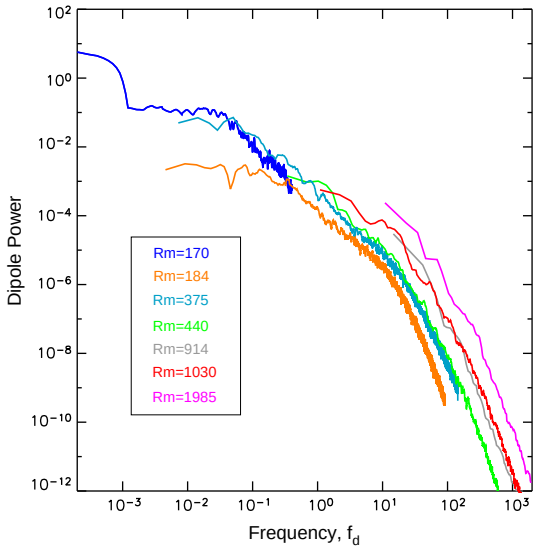

Fig. 2. Dipole power spectra from dynamos at various magnetic Reynolds numbers *Rm* with diffusive time scaling for frequency.

the spectra in Fig. 3 nearly collapse, although there remains some residual dispersion, most evident at intermediate frequencies. A portion of the residual dispersion might be removed by a proper re-scaling of the individual spectrum amplitudes, but as discussed in the previous section, we have elected not to attempt this here.

At low frequencies, the advective time scaling is nominally better than the diffusive time scaling, but here the difference between these choices is less clear-cut, in part because there are only three dynamo cases ($Rm=170$, 184 and 375) in this frequency band. Furthermore, the lowest frequency part of the $Rm=170$ spectrum is produced by a periodic variation of the outer boundary heat flow, which involves an independent external time scale that for this case is more compatible with diffusive time scaling than advective time scaling. Case *b* with $Rm=184$ is somewhat similar to the $Rm=170$ superchron cycle case *a*, but case *b* does not reverse. The comparison shows that the lack of reversals diminishes the dipole power at low frequencies but has little effect on its spectrum at higher frequencies.

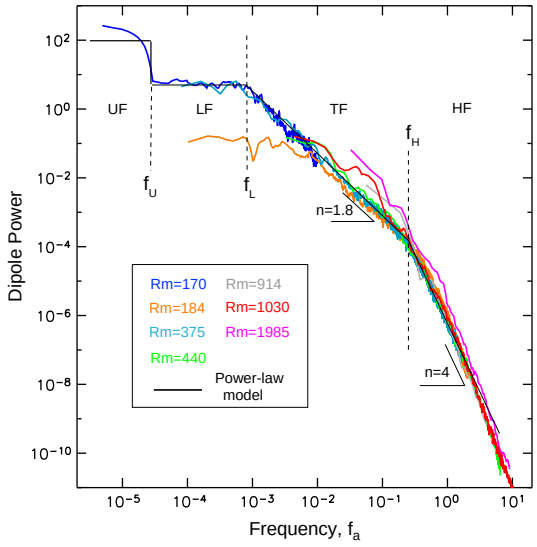

Fig. 3. Dipole power spectra from dynamos at various magnetic Reynolds numbers *Rm* with advective time scaling for frequency. Solid lines show composite power-law model from Table 2 with corner frequencies indicated by dashed lines. Slopes corresponding to power-law model exponents *n* are shown for reference.

Table 2
Power-law model for dipole frequency spectrum, cf_a^{-n}, as shown in Figs. 3–6. Percentages are the relative variance in each band for the dipole (Dp), dipole secular variation (Sv), and dipole secular acceleration (Ac) spectra.

Spectral band	Frequency range, f_a	Coefficient	Exponent	Variance,%		
		c	n	Dp	Sv	Ac
UF	$<2.5\times10^{-5}$	1×10^{2}	0	21	$\ll1$	$\ll1$
LF	$2.5\times10^{-5}-8\times10^{-4}$	5.0	0 ± 0.06	35	$\ll1$	<1
TF	$8\times10^{-4}-0.23$	1.4×10^{-5}	1.8 ± 0.1	44	46	1
HF	$0.23-5.0$	5.5×10^{-7}	4 ± 0.2	<1	53	47
VF	>5.0	1.4×10^{-5}	6 ± 0.4	$\ll1$	1	52

All of the spectra in Figs. 2 and 3 show power decreasing with frequency, but not at a consistent rate over the entire frequency range. In Fig. 3 we have divided the spectra into four bands separated by three frequencies labeled f_U, f_L, and f_H, denoting ultra-low, low, and high corner frequencies, respectively. We refer to these four as ultra-low (UF), low (LF), transitional (TF), and high (HF) frequency bands, respectively. In each of these bands we have fit the dynamo spectra to power-law models of the form cf^{-n} using least squares, where c is the coefficient and n is the exponent of the power-law discussed in Section 1. Table 2 gives best-fitting values of c and n and uncertainties for n in each band according to advective time scaling, and Fig. 3 shows their fit to the dynamo spectra. The corner frequencies were determined from the intersections of the indiviudal power-law segments. In the UF band we assumed $n=0$ a-priori. In the LF band we found $n\simeq0$ and in the HF band we found $n\simeq4$, so in our power-law model we fixed the exponents in each band to these integer values and then recalculated f_U and f_H for self-consistency.

Table 2 gives percentages of dipole variance in each band according to our power-law model. It is clear that most of the dynamo model variance resides in the UF, LF, and TF frequency bands. The most energetic is the TF band, which contains about 44% of the variance according to our power-law model, followed by the LF band that contains about 35%, and the UF band that contains most of the remainder. In contrast, the HF band contains less than 1% of the total variance. It is perhaps surprising that dipole fluctuations in numerical dynamos are so energetic at low frequencies compared to high frequencies, given that the intrinsic time scales in numerical dynamos driven by convection are relatively short. For example, the dipole free decay time, which corresponds to $f_d=1$ in Fig. 2, is often assumed to be the fundamental timescale for low frequency geomagnetic variability, yet most of the variance in our model resides at frequencies lower than this.

The power-law model exponents in Table 2 depend on the location of the spectrum corner frequencies, to some degree on the fitting method, and also on the selection of dynamo models in the stack. Because dynamo model selection necessarily involves somewhat arbitrary choices, and also because we have not applied separate scalings to the dipole amplitudes, there is some uncertainty for the model *n*-values in Table 2. Nevertheless, it is interesting to note that the LF band is nearly flat (i.e., $n\simeq0$), whereas in the TF band our power-law model has an exponent $n=1.8\pm0.1$, slightly greater than the $n=5/3$ value from classical inertial range turbulence and also slightly greater than the value reported by Sakuraba and Hamano (2007), a point that we discuss in the next section. In addition, the $n=4\pm0.2$ exponent in the HF band of our power-law model is reasonably close to although slightly higher than the $n=11/3$ value from MHD turbulence that was previously reported for the historical geomagnetic secular variation (Consolini et al., 2002).

Close inspection of the HF band in Fig. 3 reveals that the spectra show an increasingly large negative slope with increasing frequency, suggesting there may be no unique power-law exponent in the highest frequency range of our dynamos. One reason to suspect deviations

from power-law behavior in this band is the possibility of wave-induced dipole oscillations. Another reason is the damping effect of boundary layers, particularly the viscous layer beneath the outer boundary, which is much thicker in our dynamos compared to its theoretically expected thickness in the outer core. To investigate these possibilities, we extended the frequency range of the Table 1 dynamo cases *c* and *f* ($Rm=375$ and 1030, respectively) into a very high frequency (VF) band by re-sampling their dipole time series at very short intervals on the outer boundary and also below the outer boundary, at depths of 0.0381 d in the $Rm=375$ case and 0.0096 d in the $Rm=1030$ case, respectively. These depths correspond to approximately $2\sqrt{Ed}$, which is the nominal thickness of the viscous boundary layer. The resulting dipole spectra are shown in Fig. 4. Two transitions in spectral slope are evident, the first corresponding to the high frequency corner f_H at $f_a \simeq 0.23$ defined previously, and another very high frequency corner f_V evident in all spectra around $f_a \simeq 5$. In addition, the spectra measured in the dynamo interior are more energetic in the VF band compared to the spectra on the boundary, supporting the interpretation that the viscous boundary layer has a damping effect on the dipole fluctuations at very high frequencies. Note however that the slopes of the spectra on and below the outer boundary are nearly identical in the VF band. Although $n=4$ is a suitable average for the power-law exponent over the whole band, it is clear in Fig. 4 that the spectral slope increases with frequency in the VF band. A least squares fit gives a power-law exponent of $n=6\pm 0.4$ for $f_a>5$.

5. Comparison with geomagnetic dipole moment frequency spectra

Fig. 5 compares our dynamo model spectra with measured spectra of the geomagnetic dipole moment. In making this comparison we converted the power-law model in Table 2 to dimensional units with frequency scaled by the advective time in the outer core according to

$$f=\frac{f_a}{\tau_c} \tag{10}$$

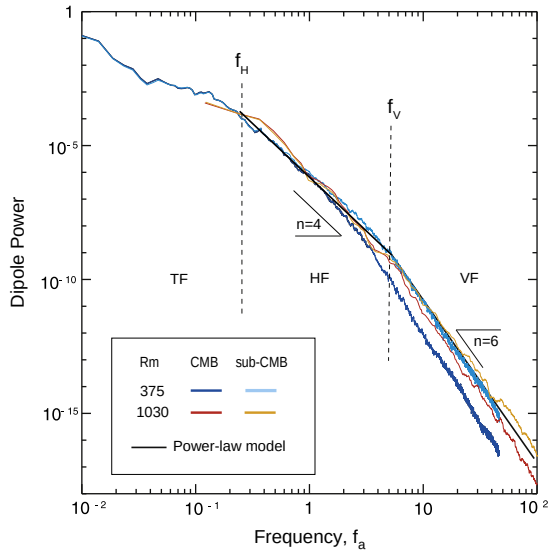

Fig. 4. High frequency behavior of dipole power spectra from dynamos at two different magnetic Reynolds numbers *Rm* with advective time scaling for frequency, measured on and below the outer boundary, denoted by CMB and sub-CMB, respectively. Solid lines show composite power-law model from Table 2 with corner frequencies f_H and f_V indicated by dashed lines. Slopes corresponding to power-law model exponents *n* are shown for reference.

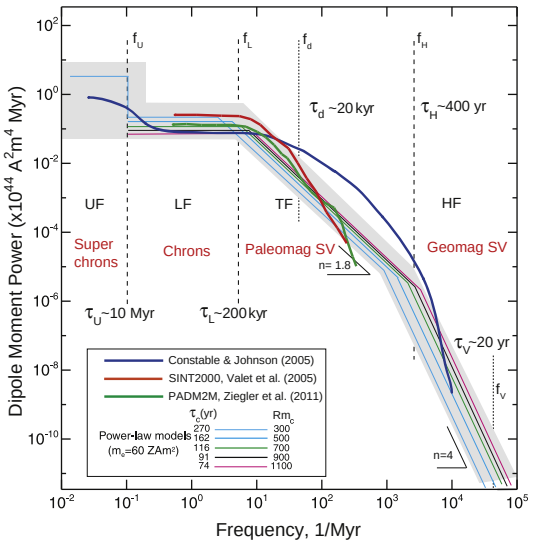

Fig. 5. Comparison of observed geomagnetic dipole moment frequency spectra (thick solid lines) with the composite power-law model from Table 2 converted to dipole moment (thin solid lines), for various outer core advection times τ_c, the shaded area denotes the range of plausible τ_c-values. Frequency bands UF, LF, TF, and HF, corner frequencies f_U, f_L, f_H, and f_V and corresponding time scales τ_U, τ_L, τ_H, and τ_V are scaled using τ_c. Rm_c is the corresponding magnetic Reynolds number and τ_d is the dipole decay time, assuming $\eta=2\ m^2\ s^{-1}$ in the outer core. Spectral slopes corresponding to power-law model exponents *n* are shown for reference.

where $\tau_c=d_c/U_c$ is the outer core advection time scale, with d_c and U_c denoting the the thickness and rms fluid velocity of the outer core. The power-law model amplitudes for $\mathcal{S}(f)$ in Fig. 5 are scaled so as to satisfy

$$\int_0^\infty \mathcal{S}df=\bar{\gamma}m_e^2 \tag{11}$$

where $m_e=60\ ZAm^2$ is the geomagnetic dipole moment averaged over the past 7 ka (Korte and Constable, 2005) and $\bar{\gamma}$ is the average ratio of the variance to mean square dipole intensity of the dynamos in Table 1. In dimensional form, the power-law model spectra disperse in proportion to the assumed value of the advection time scale in the outer core, τ_c. The magnetic Reynolds numbers $Rm_c=U_cd_c/\eta_c$ in Fig. 5 corresponding to each τ_c are shown for reference, based on $d_c=2260$ km for the outer core thickness and $\eta_c=2\ m^2s^{-1}$ for the outer core electrical conductivity, along with the approximate locations of the corner frequencies in the power-law model and f_d, the frequency that corresponds to the geomagnetic dipole free decay time.

The three spectra for the geomagnetic dipole moment in Fig. 5 are from the SINT2000 relative paleointensity record of Valet et al. (2005), the composite spectrum by Constable and Johnson (2005), and a newer composite spectrum PADM2M by Ziegler et al. (2011). The power-law model conforms to the overall shape and amplitude of the geomagnetic spectra. In particular, the highly energetic UF and LF bands in the Constable and Johnson (2005) spectrum are well represented by the model, and the increasing slope in the TF and HF bands is also present in the model. In terms of the advection time scale, the shorter advection time models (i.e., the highest Rm_c models) fit the observations somewhat better than the longer advection time models (i.e., the lower Rm_c models) particularly with regard to corner frequencies, although observed spectra are probably not precise enough to strongly favor one τ_c-value over the others. One potentially significant misfit is that the power-law models have uniform slope (constant *n*) in each band, whereas the observed geomagnetic spectra have some curvature, particularly in the TF band. For example, the Constable and Johnson (2005) composite spectrum is more

strongly curved and its contribution to the variance in the TF band exceeds that of all the power-law models. This discrepancy could be the result of too few short events in the dynamo models, but it may also be partly due to the choice of paleomagnetic relative intensity data and the methodology used to calculate the spectra, because the SINT2000 and PADM2M spectra show relatively less curvature and an overall better fit to our dynamo-based spectra, especially in the TF band. One potentially significant point of agreement concerns the low frequency corner f_L, most evident in the SINT2000 and PADM2M spectra. As seen in Fig. 3, the f_L corner is shifted toward lower frequency in dynamos with energetic low frequency dipole intensity variations and polarity reversals, compared to dynamos without reversals.

It is worth noting that neither the dynamo-based spectra nor the geomagnetic spectra in Fig. 5 show much evidence for energetic lines that might be identified with dipole oscillations. Although many types of oscillations that involve magnetic field fluctuations have been proposed for the geodynamo, such as MAC waves and torsional oscillations (Gillet et al., 2010) and external forcing by orbital variations (Thouveny et al., 2008), periodic oscillations do not seem to have an observable influence on the geomagnetic dipole intensity spectra, nor do they appear to produce large peaks in dipole intensity spectra in the numerical dynamos used in this study. Although our dynamos lack periodic external forcing, there are several types of normal modes in these dynamos that could produce dipole oscillations. In Fig. 4 for example, the inertial frequency for the $Rm=375$ dynamo is $f_a=27$ and $f_a=81$ for the $Rm=1030$ dynamo. No spectral peaks are evident at or near these frequencies, although it is possible that very weak lines have been suppressed by our filtering techniques.

6. Dipole secular variation and acceleration spectra

Figs. 6a and b show dipole secular variation and dipole secular acceleration spectra for six dynamo cases from Table 1, obtained by multiplying their dipole spectra by $(2\pi f_a)^2$ and $(2\pi f_a)^4$, respectively. The corner frequencies f_L, f_H, and f_V and our power-law model are shown for reference. The secular variation spectra in Fig. 6a have their peak power at or slightly below the high frequency corner f_H, as expected, since the average spectral exponent is less than $n=2$ in the TF band and much greater than $n=2$ in the HF band. As shown in Table 2, almost all of the variance in the dipole secular variation lies in the TF and HF bands. The low frequency corner f_L corresponds to a slope change in the dipole secular variation spectrum of the reversing $Rm=375$ dynamo, but the corresponding slope change in the non-reversing $Rm=184$ dynamo occurs at higher frequency, has reduced power in the LF band, and its spectrum has a smaller slope in the TF band, compared to the reversing dynamos. These differences can be explained by the relatively small amount of long time scale variability in the $Rm=184$ dynamo, consistent with its lack of polarity reversals and offers a possible explanation for why some dynamo spectra are closer to $n=5/3$ in the TF band (Sakuraba and Hamano, 2007).

In contrast to the dipole secular variation spectra, the dipole secular acceleration spectra in Fig. 6b have their peak power at or slightly above the high frequency corner f_H, with nearly 99% of their variance in the HF and VF bands. If the dynamo spectra in the HF and VF bands exactly followed an $n=4$ power-law, then the acceleration spectra in Fig. 6b would be flat at frequencies higher than f_H and the total variance would tend to infinity. Instead, all the acceleration spectra have broad maxima then decrease beyond f_H, demonstrating there is no unique power-law in the HF band, although the nearly symmetric (i.e., balanced) shapes of the acceleration spectra argues that $n\simeq 4$ is a good approximation to the average exponent in this band. Note that the secular acceleration spectra in Fig. 6b peak between f_H and f_V, with no systematic dependence of the peak frequency on the Rm-value. Also note that the sub-boundary spectra (denoted by s in Fig. 6b) are more energetic than their counterparts measured on the boundary for frequencies higher than f_V, although that segment of the power-law model actually fits the sub-boundary spectra better than the boundary spectra.

7. Dynamo velocity spectra

Fig. 7 shows frequency spectra for the fluctuations in rms velocity from four of the numerical dynamos in Table 1, identified by their respective Rm-values. Fig. 7a shows the velocity spectra using diffusive time scaling, and Fig. 7b shows the results for advective time scaling. These spectra were calculated from times series of the rms velocity in the outer core expressed in magnetic Reynolds number units, using the same methods as for the dipole spectra, with no separate amplitude scaling applied to the individual spectra. As found for the dipole spectra, the advective time scaling does a somewhat better job of collapsing the high frequency portions of the velocity spectra, whereas there is little to choose from between the two scalings at low frequencies. In terms of variance reduction however, neither scaling does as good a job of collapsing these velocity spectra as was found for the

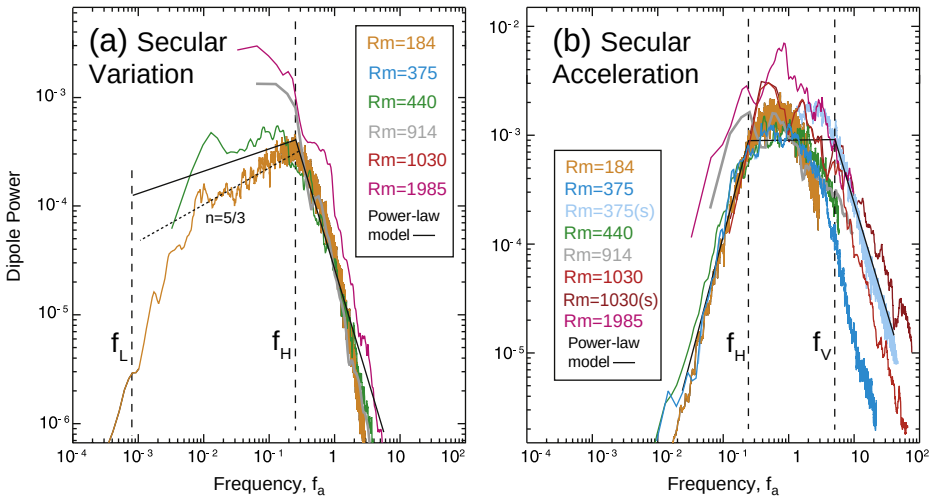

Fig. 6. Dipole secular variation (a) and dipole secular acceleration (b) spectra for dynamos at various magnetic Reynolds numbers Rm with advective time scaling for frequency. Cases labeled (s) in panel (b) are spectra measured at sub-boundary (interior) locations as described in the text. Solid lines show composite power-law model from Table 2 with corner frequencies indicated by dashed lines. The trend in the secular variation spectrum that would correspond to a power-law exponent $n=5/3$ in the dipole power spectrum is shown by a dotted line in panel (a).

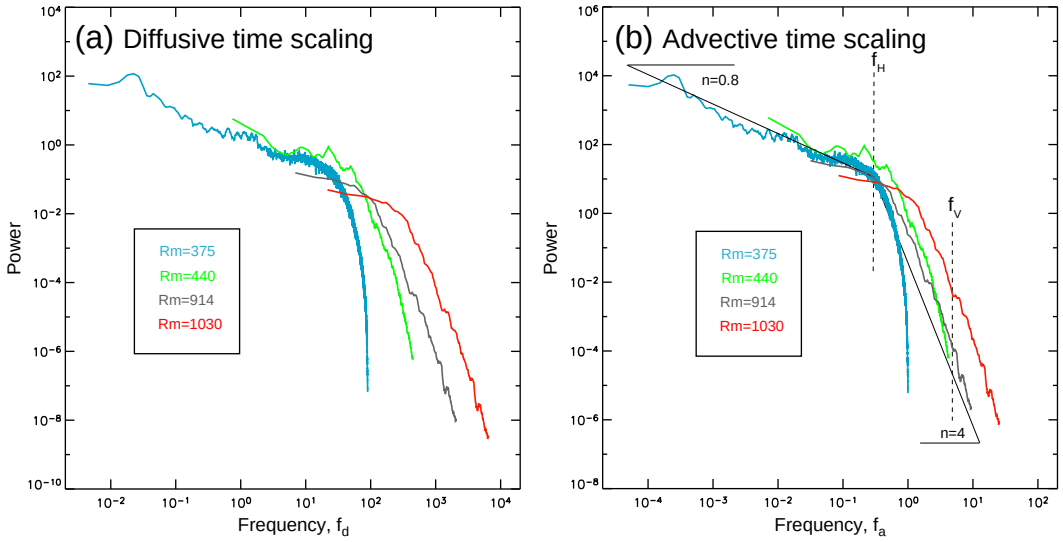

Fig. 7. Velocity power spectra from dynamos at various magnetic Reynolds numbers *Rm* using diffusive time scaling (a) and advective time scaling (b) for frequency. Representative power-law slopes and high frequency corner f_H from dipole power-law model are shown for reference.

dipole spectra. Although all the spectra in Fig. 7 show a distinct corner frequency that separates a lower frequency band with a negative slope corresponding to a power-law exponent near $n \simeq 0.8$ from a high frequency band with a large negative slope and a power-law exponent of $n = 4$ or greater, the location of the corner frequency is not tightly constrained by these spectra, nor is the slope in the high frequency band, which seems to be larger for the low *Rm* dynamos than for the high *Rm* dynamos. Even so, we see that the high frequency corner f_H for the dipole in Fig. 3 is consistent with the corner frequency in Fig. 7b, where the power in the velocity fluctuations decreases rapidly, indicating that it marks an internal time scale of the convection.

Additional information comes from the relationship between power-law exponents for velocity and magnetic field spectra. Tanriverdy and Tilgner (2011) analyzed magnetic and kinetic energy spectra in a variety of magnetohydrodynamic systems using simplified theoretical models as well as numerical calculations and found that the frequency range that corresponds to our TF band is "colored", meaning that it is characterized by a power-law exponent $n > 0$, even in cases where the kinetic energy spectrum in the same band is white, i.e. has $n \simeq 0$. Tanriverdy and Tilgner (2011) also found that in this particular frequency band the exponents of the kinetic energy and magnetic energy spectra differ by a factor of $\delta n = 2$ if the fluid velocity fluctuations are small (corresponding to laminar flow conditions), whereas $\delta n = 1$ for large velocity fluctuations (corresponding to chaotic or turbulent flow conditions). For convection-driven dynamos, they found $n \simeq 2$ for the (total) magnetic energy in the intermediate or transitional band, with $n \simeq 0$ at low Ra and $n \simeq 1$ at high Ra for the kinetic energy. For comparison, our dynamos give $n \simeq 1.8$ for the dipole part of the magnetic energy and $n \simeq 0.8$ for the kinetic energy in this band, with $\delta n \simeq 1$, consistent with the fact that our dynamos lie in the chaotic regime. Based on this, we conjecture that the frequency spectrum of kinetic energy in the outer core has the same high frequency corner f_H as the dipole, and that the slope of the kinetic energy spectrum differs from the slope of the dipole spectra in Fig. 5 by approximately $\delta n \simeq 1$ in the TF band.

8. Summary

We find that the frequency spectra of dipole fluctuations from numerical dynamos with highly diverse input parameters collapse into a consistent trend when the advection time is used for scaling frequency. Fitting the dipole spectra with this frequency scaling to a power-law model reveals at least four distinct frequency bands: (1) an ultra-low frequency band that corresponds to the repeat time between magnetic superchrons in a dynamo with slowly time-varying forcing; (2) a low frequency band that corresponds to the duration of most geomagnetic polarity chrons; (3) a transitional band that corresponds to the frequencies often recorded in sediment relative paleointensities, and (4) a high frequency band covering the historical geomagnetic secular variation. In the high frequency band the slope of the dipole spectrum increases with frequency, with the power-law exponent ranging from $n = 4$ and larger. To account for this increasing slope we include a very high frequency band in our power-law model with exponent $n = 6$. Most of the dipole variance is concentrated in the transitional, low, and ultra-low frequency bands; in contrast, the high and very high frequency bands contribute less than 1% to the dipole variance. Consistent with observed geomagnetic dipole frequency spectra, we find no obvious lines in our dynamo spectra, such as might indicate oscillations in the core that affect the dipole field intensity. Scaled to the core using realistic parameters, the amplitude and shape of our dynamo spectra are comparable to measured geomagnetic dipole moment spectra within the observational uncertainties.

Acknowledgments

We gratefully acknowledge support from grant EAR-0909622 from the Geophysics Program of the National Science Foundation. Two anonymous referees provided helpful comments.

References

Aubert, J., Labrosse, S., Poitou, C., 2009. Modeling the palaeo-evolution of the geodynamo. Geophys. J. Int. 179, 1414–1428.
Barton, C.E., 1982. Spectral analysis of paleomagnetic time-series and the geomagnetic spectrum. Philos. Trans. R. Soc. Lond. A306, 203–209.
Christensen, U., Aubert, J., 2006. Scaling properties of convection-driven dynamos in rotating spherical shells and application to planetary fields. Geophys. J. Int. 166, 97–114.
Christensen, U., Aubert, J., Hulot, G., 2010. Conditions for Earth-like geodynamo models. Earth Planet. Sci. Lett. 296, 487–496.
Consolini, G., Michelis, P., Meloni, A., 2002. Fluid motion in the Earth's core inferred from time spectral features of the geomagnetic field. Phys. Rev. E 65, 037303.
Constable, C., Johnson, C., 2005. A paleomagnetic power spectrum. Phys. Earth Planet. Inter. 153, 61–73.
Courtillot, C., Le Mouel, J.-L., 1988. Time variations of the Earth's magnetic field: from daily to secular. Annu. Rev. Earth Planet. Sci. 16, 389–476.
Curie, R.G., 1968. Geomagnetic spectrum of internal origin and lower mantle conductivity. J. Geophys. Res. 73, 2779–2790.

Driscoll, P., Olson, P., 2009. Polarity reversals in geodynamo models with core evolution. Earth Planet. Sci. Lett. 282, 24–33.
Driscoll, P., Olson, P., 2011. Superchron cycles driven by variable core heat flow. Geophys. Res. Lett. L09304. doi:10.1029/2011GL046808.
Gillet, N., Jault, D., Canet, E., Fournier, A., 2010. Fast torsional oscillations and strong magnetic field within the Earth's core. Nature 465, 74–77.
Glatzmaier, G.A., Coe, R.S., Hongre, L., Roberts, P.H., 1999. The role of the Earth's mantle in controlling the frequency of geomagnetic reversals. Nature 401, 885–890.
Guyodo, Y., Valet, J.-P., 1999. Global changes in intensity of the Earth's magnetic field during the past 800 kyr. Nature 399, 249–252.
Jackson, A., Jonkers, A.R.T., Walker, M.R., 2000. Four centuries of geomagnetic secular variation from historical records. Philos. Trans. R. Soc. Lond. A358, 947–990.
Kageyama, A., Miyagoshi, T., Sato, T., 2008. Formation of current coils in geodynamo simulations. Nature 454, 1106–1109.
Korte, M., Constable, C.G., 2005. Continuous geomagnetic field models for the past 7 millennia: 2. CALS7K. Geochem. Geophys. Geosyst. 6 (2). doi:10.1029/2004GC000801.
Olsen, N., Sabaka, T.J., Lowes, F.J., 2005. New parameterization of external and induced fields in geomagnetic modeling, and a candidate model for IGRF 2005. Phys. Planets Space 57, 1141–1149.
Olson, P., Christensen, U.R., 2006. Dipole moment scaling for convection-driven planetary dynamos. Earth Planet. Sci. Lett. 250, 561–571.
Sakuraba, A., Hamano, Y., 2007. Turbulent structure in Earth's fluid core inferred from time series of geomagnetic dipole moment. Geophys. Res. Lett. 34, L15308.
Sakuraba, A., Roberts, P., 2009. Generation of a strong magnetic field using uniform flux at the surface of the core. Nat. Geosci. 2, 802–805.
Tanriverdy, V., Tilgner, A., 2011. Global fluctuations in magnetohydrodynamic dynamos. New J. Phys. 13, 033019. doi:10.1088/1367-2630/13/3/033019.
Thouveny, N., Bourles, D.L., Saracco, G., Carcaillet, J.T., Bassionot, F., 2008. Paleoclimatic contect of geomagnetic dipole lows and excursions in the Brunhes, clue for an orbital influence on the geodynamo? Earth Planet. Sci. Lett. 275, 264–284.
Valet, J.P., Meynadier, L., Guyodo, Y., 2005. Geomagnetic dipole strength and reversal rate over the past two million years. Nature 435, 802–805.
Welch, P.D., 1967. The use of fast Fourier transform for the estimation of power spectra: a method based on time averaging over short, modified periodograms. IEEE Trans. Audio Electroacoust. AU-15, 70–73.
Ziegler, L.B., Constable, C.G., Johnson, C.L., Tauxe, L., 2011. PADM2M: a penalized maximum likelihood model of the 0–2 Ma palaeomagnetic axial dipole moment. Geophys. J. Int. 184, 1069–1089.